Chinese Chemical Letters 32 (2021) 506–510

Contents lists available at ScienceDirect

Chinese Chemical Letters

journal homepage: www.elsevier.com/locate/cclet

Communication

Fe, Cu-codoped metal-nitrogen-carbon catalysts with high selectivity and stability for the oxygen reduction reaction

Yuemin Wang[a,b,c], Ergui Luo[a,b,c], Xian Wang[a,b,c], Qinglei Meng[a,b,c], Junjie Ge[a,b,c,*], Changpeng Liu[a,b,c,*], Wei Xing[a,b,c,d,*]

[a] Laboratory of Advanced Power Sources, Changchun Institute of Applied Chemistry, Chinese Academy of Sciences, Changchun 130022, China
[b] University of Science and Technology of China, Hefei 230026, China
[c] Jilin Province Key Laboratory of Low Carbon Chemical Power Sources, Changchun 130022, China
[d] State Key Laboratory of Electroanalytical Chemistry, Changchun Institute of Applied Chemistry, Chinese Academy of Sciences, Changchun 130022, China

ARTICLE INFO

Article history:
Received 21 February 2020
Received in revised form 17 March 2020
Accepted 23 March 2020
Available online 27 March 2020

Keywords:
Fuel cell
Oxygen reduction reaction
Fe, Cu-codoped metal-nitrogen-carbon catalysts
High selectivity
High stability

ABSTRACT

Metal-nitrogen-carbon materials (M-N-C) are non-noble-metal-based alternatives to platinum-based catalysts and have attracted tremendous attention due to their low-cost, high abundance, and efficient catalytic performance towards the oxygen reduction reaction (ORR). Among them, Fe-based materials show remarkable ORR activity, but they are limited by low selectivity and low stability. To address these issues, herein, we have synthesized FeCu-based M-N-C catalysts, inspired by the bimetal center of cytochrome c oxidase (CcO). In acidic media, the selectivity was notably improved compared with Fe-based materials, with peroxide yields less than 1.2% (<1/3 of the hydrogen peroxide yields of Fe-N-C catalysts). In addition to Cu-N-C catalysts which can catalytically reduce hydrogen peroxide, the reduction current of hydrogen peroxide using FeCu-N-C-20 exceeded that of Fe-N-C by about 6% when the potential was greater than 0.4 V. Furthermore, FeCu-based M-N-C catalysts suffered from only a 15 mV attenuation in their half-wave potentials after 10,000 cycles of accelerated degradation tests (ADT), while there was a 30 mV negative shift for Fe-N-C. Therefore, we propose that the H_2O_2 released from Fe-N_x sites or N-doped carbon sites would be reduced by adjacent Cu- N_x sites, resulting in low H_2O_2 yields and high stability.

Oxygen reduction is one of the most important electrochemical reactions due to its broad applications in energy conversion processes, including metal-air batteries and fuel cells [1–7]. Due to the high costs of platinum-based catalysts, there is a need for cheaper alternatives with similar catalytic performances. Among non-platinum catalysts, metal-nitrogen-carbon (M-N-C) materials have attracted much attention due to their excellent performances and low-cost; however, M-N-C catalysts still have much lower ORR performances than Pt-based catalysts [8–11].

In M-N-C materials, it is widely accepted that the ORR active sites are M-N_x sites, where x = 2 or 4, and M represents Fe or Co [12–14]. In order to enhance the ORR performance, except different nonmetal dopants, such as phosphorus and sulfur [15–20], it is also effective to develop multimetal-based M-N-C catalysts. Even though the synergistic effects between different metals are well-known, there are few literature reports about multimetal-codopants, aside from Fe/Co and Fe/Mn [1,21]. These studies have typically focused upon improving the ORR activity and have neglected the influence of multimetal-codopants on the selectivity and stability. And it is widely known that OH radicals released through a Fenton reaction can destroy proton-exchange membranes and catalysts [22,23]. Therefore, in addition to activity, there is a need to improve the electrochemical selectivity and stability of catalysts for the ORR.

Various enzymes are used in nature to effectively convert substrates under mild conditions; therefore, the structures and components of corresponding enzymes provide important references to design and synthesize artificial catalysts [24]. Cytochrome c oxidase (CcO) is an important enzyme that possesses an a3-CuB site, in which an oxygen molecule is bridged and then cleaved [25–27] or in which CuB serves as electron storage [28]. Although it is difficult to illuminate the mechanism, mimicking such an enzyme is still beneficial for developing high-performancecatalysts, and

* Corresponding authors at: Laboratory of Advanced Power Sources, Changchun Institute of Applied Chemistry, Chinese Academy of Sciences, Changchun 130022, China.
E-mail addresses: gejj@ciac.ac.cn (J. Ge), liuchp@ciac.ac.cn (C. Liu), xingwei@ciac.ac.cn (W. Xing).

https://doi.org/10.1016/j.cclet.2020.03.061
1001-8417/

feedback from biomimetic catalytic phenomena may aid in clarifying the catalytic mechanism. Additionally, enzymes possess some disadvantages, such as sensitivity to temperature, air, pH and moisture, and difficult separation from products. Therefore, mimicking enzyme active sties to construct heterogeneous catalysts containing Fe and Cu, *i.e.*, FeCu-bimetal-based M-N-C materials, is an effective strategy to overcome such disadvantages.

Herein, we adopted FeCu-Prussian blue analogues (FeCu-PBAs) in which Fe and Cu cations are linked by CN- [29], as metal precursors to synthesize M-N-C materials, in which mildly oxidized BP-2000 (MOBP) and melamine served as the carbon and nitrogen sources, respectively (Scheme 1). Heterogeneous metal-based FeCu-N-C-x, where x refers to the FeCu-PBA contents added into the initial precursor mixture, were prepared by mimicking the CcO components. FeCu-based materials possessed much higher selectivities and stabilities than Fe-N-C, while the reduction current of hydrogen peroxide using FeCu-based materials exceeded that of Fe-N-C by about 6% when the potential was greater than 0.4 V. Therefore, a cascade reaction mechanism for ORR was proposed in which H_2O_2 released from Fe-N_x sites or N-doped carbon sites was reduced by adjacent Cu-N_x sites, which resulted in low H_2O_2 yields and high stability.

Scanning electron microscopy (SEM) and transmission electron microscopy (TEM) were used to obtain morphological information. FeCu-N-C-x materials maintained the initial oxidized BP-2000 morphology in the SEM images (Fig. S1 in Supporting information). And the catalyst structure varies with the metal content, including Fe, Co and Ni [10,11,30–32]. Herein, at relatively high contents, metal-encapsulated catalysts are formed, which are important branches of M-N-C catalysts and deserve a lot of research. And the catalytic activity is similar to that of atomically distributed catalysts, but more stable due to encapsulation structure. When decreasing metal contents, metallic elements were well-dispersed throughout the carbon matrix in the form of atoms or clusters, and no encapsulation structures were formed. The ICP results (Table S1 in Supporting information) showed that the metal contents of the prepared catalysts could reach up to 0.67 wt% for Fe and 0.1 wt% for Cu, and metal nanoparticles encapsulated by a few layers of graphene appeared in FeCu-N-C-25 materials (Fig. S2 in Supporting information). The similar morphologies helped eliminate the influence of morphology, which provided a better understanding of the relationship between other intrinsic factors, such as metal content, nitrogen content, and pore structures and performance. Furthermore, metal dispersion is also critical for the catalytic performance. The transmission electron microscopy (TEM) images and corresponding element mappings indicated that the metals and nitrogen were well-dispersed throughout the carbon matrix, which was advantageous for the formation of metal-N_x active sites (Fig. 1 and Fig. S3 in Supporting information).

A large specific surface area also improves catalytic performance [32–36], and larger surface areas expose more active sites, resulting in a better catalytic activity. Furthermore, a large pore

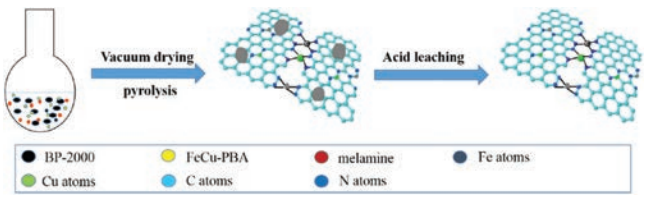

Scheme 1. Schematic diagram of the synthesis of FeCu-N-C catalysts. After the pyrolysis of carbon, nitrogen, and metal sources, metal nanoparticles formed in the mixture. The metal nanoparticles were etched by acidic leaching, and Fe-N_x and Cu-N_x sites were maintained (black circles refer to BP-2000, yellow FeCu-PBA, red melamine, and gray atoms refer to Fe, green Cu, cyan atoms C, blue N).

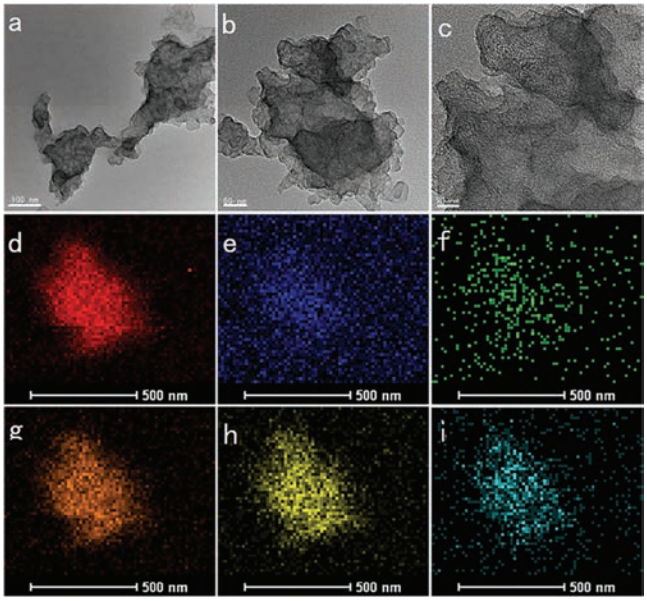

Fig. 1. (a-c) Transmission electron microscopy (TEM) images of FeCu-N-C-20, and the scale bars are 100, 50 and 20 nm, respectively. EDX elemental mappings of (d) C-K, (e) Cu-K, (f) Fe-K, (g) N-K, (h) O-K and (i) Fe-L, which correspond to HAADF-STEM image of FeCu-N-C-20 catalyst in Fig. S3 (Supporting information).

width is favorable for mass transport, including oxygen, protons, and water. As indicated by physical sorption experiments (Table S2 in Supporting information), the catalysts possessed extraordinarily high specific surface areas (950−1200 m^2/g) and pore widths (3.3 nm) due to the presence of the same carbon matrix. Thus, the mass transport limitation was alleviated efficiently.

The XRD patterns of FeCu-N-C-x were shown in Fig. 2. Due to the low metal contents (< 0.67 wt% Fe by ICP), all prepared catalysts possessed two broad peaks (near 25° and 45°), which were assigned to carbon materials, and no metal or metal carbide peaks were visible even for FeCu-N-C-25 materials. X-ray photoelectron spectroscopy (XPS) is an effective method to investigate the surface elemental composition, where C, N and O were present in the catalysts, while no peaks attributed to Fe and Cu were observed due to their low metal contents, in accordance with the ICP results (Table S1). Metals are essential for the formation of active sites and catalytic performance. We showed that metal contents increased with the initial metal precursors (from 0.058 wt% to 0.67 wt% for Fe) (Table S1). Even for FeCu-N-C-20, the Fe and Cu metal contents can be low to 0.64 wt% and 0.12 wt %, respectively. In addition, we also investigated the N 1s peaks, which indicated that the nitrogen contents of all catalysts were between 0.76 at% and 2.78 at%. The N 1s peaks of the high-resolution XPS spectra were deconvoluted into five peaks: pyridinic N, metal-N_x, pyrrolic N, graphitic N, and N oxide [8,30,31,37,38]. For FeCu-N-C-20, the percent of pyridinic N and metal-N_x was the highest among the catalysts, which are usually considered to be the active components of active sites (Table S1 and Fig. S4 in Supporting information).

The electrochemical performances of the prepared catalysts were tested through the rotating disk electrode (RDE) and rotating ring disk electrode (RRDE) in 0.1 mol/L $HClO_4$ solution. Tafel plots were used to evualate the kinetics of the ORR, in which lower Tafel slopes indicate faster kinetics. In acidic media, the performance of FeCu-N-C-20 surpassed the other FeCu-N-C catalysts, whose half-wave potentials reached 0.784 V, which was still lower than that of Pt/C (0.882 V) (Fig. S5 in Supporting information). As the metal

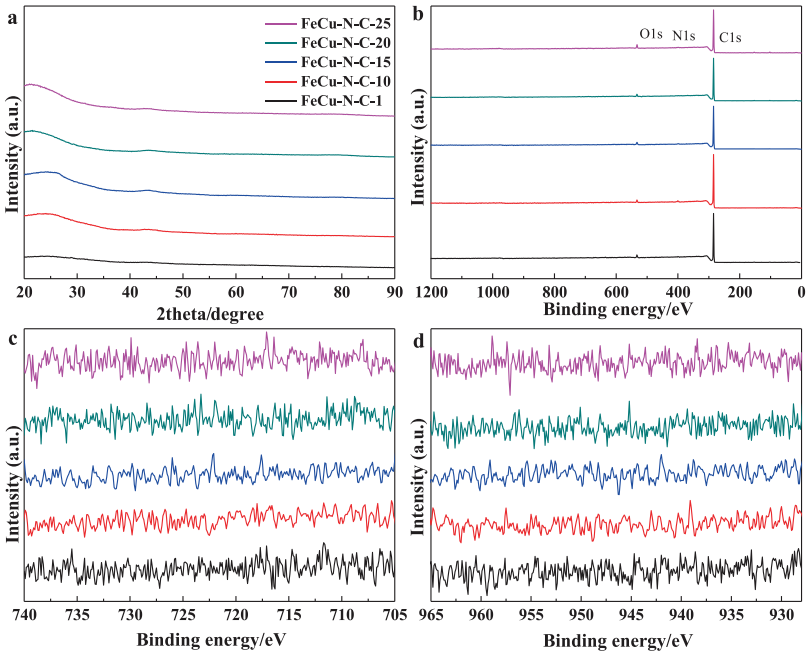

Fig. 2. (a) XRD patterns and (b)XPS survey scans of FeCu-N-C-x (x = 1, 10, 15, 20, and 25). The high-resolution XPS spectra of (c) Fe 2p and (d) Cu 2p of FeCu-N-C-x (x = 1, 10, 15, 20 and 25).

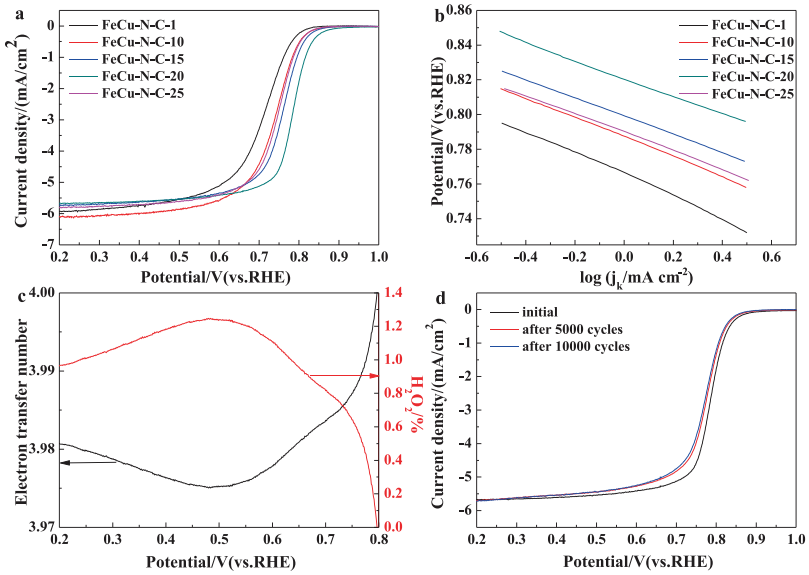

Fig. 3. ORR performance of FeCu-N-C-x (x = 1, 10, 15, 20, 25) in 0.1 mol/L $HClO_4$ solution. (a) LSV curves of FeCu-N-C-x with 1600 rpm and 10 mV/s in an oxygen-saturated acidic solution, and a catalyst loading of 0.5 mg/cm^2. (b) Tafel plots for FeCu-N-C-x according to the data of (a). (c) Electron transfer number and H_2O_2 yields of FeCu-N-C-20 in an acidic media, respectively. (d) ORR curves of FeCu-N-C-20 before and after 5,000 and 10,000 cycles in an oxygen-saturated acidic solution.

contents increased, the Tafel slopes varied from 63 mV/dec to 51 mV/dec, and then increased to 53 mV/dec. (Fig. 3a, and b)The decrease of the Tafel slopes was due to the increased metal loading, however, for FeCu-N-C-25 catalysts, the high-loading metal formed metal nanoparticles instead of Fe- N_x sites, leading to increased Tafel slope. And the Tafel slope of FeCu-N-C-20 (51 mV/dec) was lower than that of Pt/C (62.8 mV/dec). Furthermore, the ultralow H_2O_2 yield (<1.2%) indicated that oxygen was reduced to water *via* a 4-electron pathway. (Fig. 3c)

Stability is another important catalyst characteristic and is correlated with H_2O_2 yield because hydroxyl radicals generated from peroxides can oxidize carbon materials and destroy active sites. A 22 mV attenuation was observed in the half-wave potential of Pt/C after 10,000 cycles, and there was only a 15 mV shift from 0.784 V (11 mV and 15 mV negative shift after 5,000 and 10,000 cycles, Fig. 3d). Such phenomena demonstrated that FeCu-N-C-20 catalysts possess good stability in acidic media.

To better understand the influence of Fe and Cu dopants on ORR performance, Fe-N-C and Cu-N-C catalysts were prepared and tested with FeCu-N-C-20 catalysts in acidic media, respectively. The catalysts both possessed similar physical properties (Fig. S6 in Supporting information). The half-wave potential and Tafel slope of FeCu-N-C-20 were nearly the same as Fe-N-C, but differences were evident in the peroxide yields (Figs. 4a and b). The H_2O_2

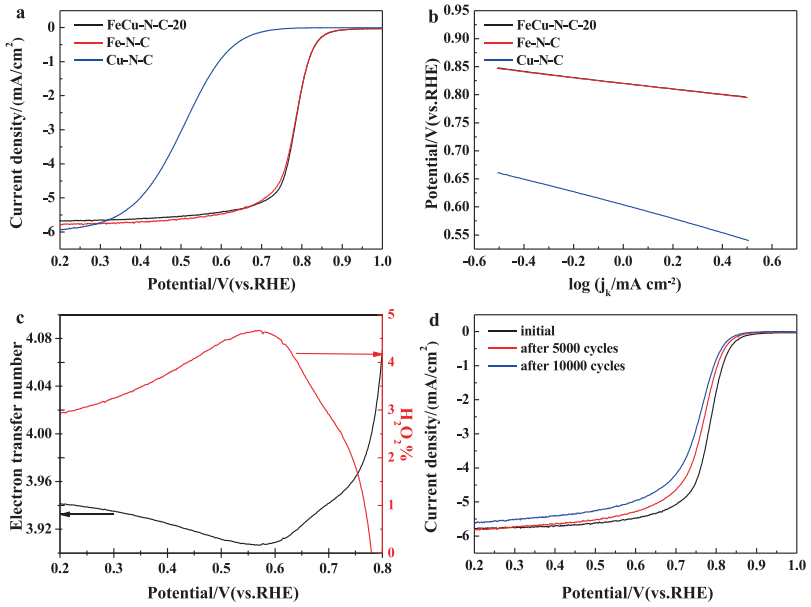

Fig. 4. ORR performance of FeCu-N-C-20, Fe-N-C and Cu-N-C in 0.1 mol/L $HClO_4$ solution. (a) LSV curves of FeCu-N-C-20, Fe-N-C and Cu-N-C with 1600 rpm and 10 mV/s in an oxygen-saturated acidic solution, and catalyst loadings of 0.5 mg/cm^2. (b) Tafel plots of FeCu-N-C-20, Fe-N-C and Cu-N-C according to the data of (a). (c) Electron transfer number and H_2O_2 yields of Fe-N-C in acidic media, respectively. (d) ORR curves of Fe-N-C before and after 5,000 and 10,000 cycles in an oxygen-saturated acidic solution.

yields of Fe-N-C reached 4.7% at around 0.57 V (Fig. 4c), while the H_2O_2 yields of FeCu-N-C-20 were less than 1.2%, which were less than 1/3 of the hydrogen peroxide yields of Fe-N-C catalysts, suggesting that bimetal-based catalysts effectively decrease peroxide yields. [39,40] In addition, Fe-N-C suffered from a 19 mV and 30 mV attenuation in the half-wave potential after 5,000 and 10,000 cycles ADTs (Fig. 4d), while only 11 mV and 15 mV negative shifts in the half-wave potential were observed for FeCu-N-C-20, implying that FeCu-N-C-20 possess excellent stability. We could not clearly conclude that Fe-doping and Cu-doping were still present in the structure in the same relative positions as in FeCu-PBA materials; however, the aforementioned results confirmed that the synergistic effects between Fe and Cu helped suppress peroxide formation. Thus, FeCu bimetal-based catalysts possessed excellent selectivity and stability.

Since proton exchange membrane fuel cells operate under acidic conditions, this paper focuses on gaining insight into comprehensively understanding the electrocatalytic mechanism in acid. Here, an electrochemical method was employed to calculate the active site density and turnover frequency (TOF) of different catalysts based upon the nitrite reduction reaction in weakly acidic solution (Table S3 and Figs. S7-S9 in Supporting information) [41]. The active site density is directly correlated with metal sites accessible and is determined by integrating nitrite reduction currents. For Fe-N-C and Cu-N-C, the sum of the metal contents detected *via* the electrochemical method was similar to the metal content of FeCu-N-C-20. Additionally, the TOF value of Cu-N-C was negligible compared with Fe-N-C (0.02/s for Cu-N-C *vs.* 3.7/s for Fe-N-C; about 185 times that of Cu-N-C). Therefore, when calculating the TOF of FeCu-N-C-20, we simply accounted for Fe-related active sites. Due to the similar ORR activity and active site density, the TOF values were nearly identical for Fe-N-C and FeCu-N-C-20 (3.7/s and 3.56/s), which indicates that Cu-doping does not affect the oxygen reduction activity.

The function of the Cu dopant was then investigated by electrochemically testing the three materials in a mixed solution containing 0.1 mol/L $HClO_4$ and 1.3 mmol/L H_2O_2. The LSV curve of Cu-N-C was nearly linear when the potential was less than 0.8 V, and the H_2O_2 reduction current of FeCu-N-C-20 was greater than that of Fe-N-C by about 6%–20% (Fig. S10 in Supporting information). Consequently, the Cu dopant effectively participated in the peroxide reduction indicating why FeCu-N-C-20 displayed a lower H_2O_2 yield and higher stability than Fe-N-C. These phenomena implied that adjacent Fe-N_x, N-C and Cu-N_x sites led to oxygen cascade reactions, *i.e.*, peroxides generated from Fe-N_x sites and N-C sites were consumed by adjacent Cu-N_x sites, which resulted in low H_2O_2 yields and high stability.

Here, we have synthesized a high-performance and low-cost FeCu-N-C catalyst for ORR. The half-wave potential and limiting current density reached 0.784 V and 5.88 mA/cm^2 in acidic media, respectively. A notably higher selectivity and stability were realized compared with Fe-N-C. In contrast, there were no observed activity differences, as verified by turnover frequencies (TOF) through electrochemical methods. In addition, Cu-N-C displayed catalytic reduction capabilities for hydrogen peroxide, and the H_2O_2 reduction current of FeCu-N-C-20 was greater than that of Fe-N-C by about 6%– 20%. Therefore, we propose that oxygen reacts through a 2-electron or 4-electron pathway at Fe-N_x sites or N-doped carbon sites. Then H_2O_2 released from these sites is reduced by adjacent Cu-N_x sites, resulting in a low H_2O_2 yield and high stability. This nature-inspired design strategy paves a way to synthesize catalysts by mimicking corresponding natural functional oxidases.

Declaration of competing interest

The authors declare that they have no known competing financial interests or personal relationships that could have appeared to influence the work reported in this paper.

Acknowledgments

The authors thank the National Science and Technology Major Project (No. 2017YFB0102900), the National Natural Science Foundation of China (Nos. 21633008,21433003), the Jilin Province Science and Technology Development Program

(No. 20170203003SF), and the Hundred Talents Program of the Chinese Academy of Sciences for financial support.

Appendix A. Supplementary data

Supplementary material related to this article can be found, in the online version, at doi:https://doi.org/10.1016/j.cclet.2020.03.061.

References

[1] G. Wu, K.L. More, C.M. Johnston, P. Zelenay, Science 332 (2011) 443–447.
[2] M. Lefèvre, E. Proietti, F. Jaouen, J.P. Dodelet, Science 324 (2009) 71–74.
[3] D. Wang, H.L. Xin, R. Hovden, et al., Nat. Mater. 12 (2013) 81–87.
[4] J. Greeley, I.E.L. Stephens, A.S. Bondarenko, et al., Nat. Chem. 1 (2009) 552–556.
[5] M. Shao, Q. Chang, J.P. Dodelet, R. Chenitz, Chem. Rev. 116 (2016) 3594–3657.
[6] Y. Yang, Y. Tang, H. Jiang, et al., Chin. Chem. Lett. 30 (2019) 2089–2109.
[7] B. Wang, X. Cui, J. Huang, R. Cao, Q. Zhang, Chin. Chem. Lett. 29 (2018) 1757–1767.
[8] C. Zhu, S. Fu, J. Song, et al., Small 13 (2017) 1603407.
[9] T. Liu, P. Zhao, X. Hua, et al., J. Mater. Chem. A 4 (2016) 11357–11364.
[10] Q. Wang, K. Ye, L. Xu, et al., Chem. Commun. 55 (2019) 14801–14804.
[11] Z. Chen, Q. Wang, X. Zhang, et al., Sci. Bull. 63 (2018) 548–555.
[12] H. Schulenburg, S. Stankov, V. Schunemann, et al., J. Phys. Chem. B 107 (2003) 9034–9041.
[13] F. Charreteur, F. Jaouen, S. Ruggeri, J.P. Dodelet, Electrochim. Acta 53 (2008) 2925–2938.
[14] M. Lefevre, E. Proietti, F. Jaouen, J.P. Dodelet, Science 324 (2009) 71–74.
[15] Z. Yang, Z. Yao, G. Li, et al., ACS Nano 6 (2012) 205–211.
[16] L. Xu, G. Pan, X. Liang, RSC Adv. 4 (2014) 19756–19765.
[17] K. Hu, L. Tao, D. Liu, J. Huo, S. Wang, ACS Appl. Mater. Interfaces 8 (2016) 19379–19385.
[18] X. Zheng, Z. Yang, J. Wu, et al., RSC Adv. 6 (2016) 64155–64164.
[19] W. Yang, L. Chen, X. Liu, et al., J. Mater. Chem. A 4 (2016) 5834–5838.
[20] C. Li, Z. Chen, Y. Ni, et al., J. Mater. Chem. A 4 (2016) 14291–14297.
[21] M. Kuang, Q. Wang, P. Han, G. Zheng, Adv. Energy Mater. 7 (2017) 1700193.
[22] C.H. Choi, H.K. Lim, M.W. Chung, et al., Energy Environ. Sci. 11 (2018) 3176–3182.
[23] Y. He, S. Hwang, D.A. Cullen, et al., Energy Environ. Sci. 12 (2019) 250–260.
[24] F. Moller, S. Piontek, R.G. Miller, U.P. Apfel, Chem. Eur. J. 24 (2018) 1471–1493.
[25] S. Ferguson-Miller, G.T. Babcock, Chem. Rev. 96 (1996) 2889–2908.
[26] F. Poiana, C. von Ballmoos, N. Gonska, et al., Sci. Adv. 3 (2017) e1700279.
[27] P.R. Rich, Biochem. Soc. Trans. 45 (2017) 813–829.
[28] J.P. Collman, R. Boulatov, C.J. Sunderland, L. Fu, Chem. Rev. 104 (2004) 561–588.
[29] Y. Wang, S. Bao, R. Li, et al., ACS Appl. Mater. Interfaces 7 (2015) 2088–2096.
[30] J. Zhu, M. Xiao, Y. Zhang, et al., ACS Catal. 6 (2016) 6335–6342.
[31] J. Zhu, M. Xiao, C. Liu, et al., J. Mater. Chem. A 3 (2015) 21451–21459.
[32] J. Liu, T. He, Q. Wang, et al., J. Mater. Chem. A 7 (2019) 12451–12456.
[33] S. Barazzouk, M. Lefevre, J.- Dodelet, J. Electrochem. Soc. 156 (2009) B1466–B1474.
[34] V.R. Stamenkovic, B. Fowler, B.S. Mun, et al., Science 315 (2007) 493–497.
[35] U.A. Paulus, A. Wokaun, G.G. Scherer, et al., Electrochim. Acta 47 (2002) 3787–3798.
[36] W. Liu, M. Zhu, J. Liu, X. Li, J. Liu, Chin. Chem. Lett. 30 (2019) 750–756.
[37] J. Zhu, K. Li, M. Xiao, et al., J. Mater. Chem. A 4 (2016) 7422–7429.
[38] M. Xiao, J. Zhu, L. Feng, C. Liu, W. Xing, Adv. Mater. 27 (2015) 2521–2527.
[39] J.C. Li, F. Xiao, H. Zhong, et al., ACS Catal. 9 (2019) 5929–5934.
[40] X.X. Wang, V. Prabhakaran, Y. He, Y. Shao, G. Wu, Adv. Mater. 31 (2019) 1805126.
[41] D. Malko, A. Kucernak, T. Lopes, Nat. Commun. 7 (2016) 13285.